PAPER

Check for updates

Oriented exchange-coupled L1$_0$-FePt/Co core-shell nanoparticles with variable Co thickness†

Xin Liu, [ID] Shulan Zuo, Hui Wang, Tianli Zhang, Ying Dong [ID] and Chengbao Jiang*

Exchange-coupled core–shell nanoparticles are expected to be the new generation of permanent magnets, where the orientation of the hard magnetic phase is supposed to play a key role in improving their magnetic performance. In this work, L1$_0$-FePt/Co core–shell nanoparticles with Co thickness ranging from 0.6 to 2.2 nm have been synthesized by a seed-mediated growth method. The exchange coupling effect between the hard core and soft shell led to a 60% improvement of the maximum magnetic energy product ((BH)$_{max}$), compared with the pure L1$_0$-FePt core. By tuning the amount of precursor, nanoparticles with different Co shell thicknesses were synthesized. Furthermore, the L1$_0$-FePt/Co core–shell nanoparticles were dispersed in epoxy resin and oriented under an external magnetic field. The (BH)$_{max}$ of the anisotropic nanocomposite magnet with a Co thickness of 1 nm is 7.1 MGOe, enhanced by 117% compared with the isotropic L1$_0$-FePt magnet, which paves the way for the development of high-performance permanent magnets for energy conversion applications.

Introduction

Over the past few decades, the growing demands for motors applied in electric vehicles and wind-driven generators have impelled the improvement of the maximum magnetic energy product ((BH)$_{max}$) of permanent magnets.[1–4] Conventional high-performance permanent magnets such as Nd$_2$Fe$_{14}$B and Sm$_2$Co$_{17}$ are increasingly constrained by the scarcity of rare earths.[5–7] Consequently, there is a need to exploit an alternative magnet.[8–10] The exchange-coupled nano-magnets with the advantages of both hard and soft magnetic phases have the potential to achieve high (BH)$_{max}$ with little or even no rare earth.[11–13] Since Skmoski and Coey predicted that the (BH)$_{max}$ of exchange-coupled magnets could reach 120 MGOe in 1993,[14] considerable efforts have been made to improve (BH)$_{max}$ of exchange coupled magnets. However, the practical (BH)$_{max}$ is far below the theoretical prediction up to now. For achieving performance breakthroughs, the orientation of the hard magnetic phase is considered to be an effective method.

Hard magnetic L1$_0$-FePt nanoparticles prepared by the wet chemical method[15–18] have large magnetocrystalline anisotropy, small superparamagnetic critical size, controllable shape, catalytic activity, and can be aligned by a magnetic field.[19,20] They are often used as building blocks of exchange-coupled magnets such as FePt/Fe$_3$Pt,[21,22] FePt/Co,[23–25] FePt/Fe,[26] FePt/FeCo,[27,28] and FePt/Fe$_3$O$_4$.[15,23,29,30] Exchange-coupled FePt/Co

core–shell nanoparticles with controllable Co thickness was prepared by Liu *et al.* for the first time,[23] where the introduction of the soft phase increased the saturation magnetization (M_s) of the nanoparticles. However, compared with L1$_0$-FePt nanoparticles, due to the exchange coupling effect, the hardness of L1$_0$-FePt/Co core–shell nanoparticles is reduced, which makes the orientation of nanoparticles difficult.[31] Our previous work shows that L1$_0$-FePt/Co nanoparticles can be aligned under a magnetic field, but the magnetic shielding effect caused by the agglomeration of nanoparticles hindered the process of orientation.[25]

In this work, Co was chosen for its high M_s to construct the exchange-coupled core–shell nanoparticles with L1$_0$-FePt. The (BH)$_{max}$ of L1$_0$-FePt nanoparticles can be increased to a certain extent by Co coating. But the introduction of soft magnetic phase makes the orientation of nanoparticles difficult. Therefore, we need to find a critical point where the orientation of the nanoparticles is not so difficult, but also allow a certain increase in magnetic remanence, and finally the maximum (BH)$_{max}$ was obtained. This needs to find the best thickness value by adjusting the thickness of Co. In this work, different thicknesses of Co shell were coated on the surface of the L1$_0$-FePt nanoparticles by seed-mediated growth method.[25] Furthermore, the anisotropic magnets were prepared by fixing the L1$_0$-FePt/Co core–shell nanoparticles in uncured epoxy resin under an external magnetic field, where the agglomeration problem was solved by the method proposed in our last work.[19] The nanoparticles with different Co thicknesses were prepared to study the orientation of exchange-coupled nanoparticles. The (BH)$_{max}$ of 7.1 GMOe is obtained in the anisotropic L1$_0$-FePt/Co magnet with a Co thickness of 1 nm, topping out at 217% of the isotropy magnet.

School of Materials Science and Engineering, Beihang University, Beijing 100191, P. R. China. E-mail: jiangcb@buaa.edu.cn

Experimental

Materials

Platinum acetylacetonate [Pt(acac)$_2$, purity 97%], magnesium acetylacetonate [Mg(acac)$_2$·2H$_2$O, purity 98%], cobalt acetylacetonate [Co(acac)$_2$, purity 97%], oleylamine (OAm, 70%) and oleic acid (OA, 90%) was purchased from Sigma Aldrich. Pentacarbonyl iron [Fe(CO)$_5$ purity 99%], nitric acid(HNO$_3$, concentration 68%), methylbenzene(purity 99%) and absolute ethyl alcohol was purchased from Beijing Chemical Works. All chemicals were used as received.

Preparation of L1$_0$-FePt/Co core–shell nanoparticles

Synthesis of fct-FePt/MgO nanoparticles. L1$_0$-FePt nanoparticles were synthesized by using the method reported by Sun.[32,33] It can be simply summed up as three steps. Firstly, fcc-FePt nanoparticles were synthesized by a wet chemistry method that involved decomposition and reduction of Pt(acac)$_2$ and Fe(CO)$_5$. Secondly, by decomposing Mg(acac)$_2$·2H$_2$O, a Mg layer was coated on the surface of fcc-FePt nanoparticles. The unstable Mg was oxidized to MgO by the oxygen in the air. Thirdly, the nanoparticles transform from the fcc phase to the fct phase by annealing at 700 °C for 6 h.

Preparation of L1$_0$-FePt nanoparticles. 0.04 g L1$_0$-FePt/MgO nanoparticles were ultrasonically dispersed in 50 ml alcohol with the presence of OAm and OA. 2 ml HNO$_3$ was then added dropwise to remove MgO. The solution was ultrasonically stirred for 5 min and then was centrifugally cleaned by alcohol and acetone 5 times. The obtained L1$_0$-FePt nanoparticles were dispersed in 5 ml toluene added with OAm and OA as surfactants.

Synthesis of L1$_0$-FePt/Co core–shell nanoparticles. For Co layer thickness of 2 nm, the preparation method of L1$_0$-FePt/Co nanoparticles was as follows. 0.06 g L1$_0$-FePt/MgO nanoparticles were acid pickled by 2 ml HNO$_3$ in 50 ml alcohol with the presence of OAm and OA. The sediment was centrifugal cleaned by acetone 5 times, and then it was dissolved in 5 ml toluene for later use. 11 mg Co(acac)$_2$ was dissolved in 30 ml OAm in a four flask. The solution was heated to 100 °C under a flow of 5% H$_2$ and 95% Ar, stirred constantly. L1$_0$-FePt/MgO nanoparticles dispersed in 5 ml methylbenzene were injected into the four flasks. After toluene evaporation, the solution was slowly heated to 300 °C and kept for 1 h. Then the solution was cooled down to room temperature. The production was centrifugally cleaned by acetone and alcohol 5 times. The L1$_0$-FePt/Co core–shell nanoparticles were dispersed in 5 ml methylbenzene with the presence of OAm and OA.

Orientation

1 mg L1$_0$-FePt or L1$_0$-FePt/Co core–shell nanoparticles were dispersed in 0.5 ml epoxy. After stirring for 1 h, 0.5 ml curing agent was added to the mixture. Before the epoxy solidifying, the composite was transferred into a permanent magnet's cavity with a magnetic field of 2 T. The anisotropic L1$_0$-FePt/Co-based exchange-coupled nano-magnet was obtained after the epoxy solidified, as shown in Fig. S1.†

Characterization

Transmission electron microscopy (TEM) and high-resolution transmission electron microscopy (HRTEM) imaging of nanoparticles were performed on a JEOL 2100F with an accelerating voltage of 200 kV. TEM samples were prepared by dropping toluene dissolved nanoparticles on the corban grids. The magnetic properties of nano-magnets were evaluated using a physical property measurement system (PPMS, Quantum Design Co., Ltd, USA).

Results and discussion

L1$_0$-FePt nanoparticles were synthesized by a wet chemical method. The decomposition of Fe(CO)$_5$ and the reduction of Pt(acac)$_2$ led to the formation of superparamagnetic fcc-FePt nanoparticles. The ferromagnetic fct-FePt nanoparticles were obtained by annealing these fcc-FePt nanoparticles at 700 °C.[32,34] To prevent the nanoparticles from oxidation, a shell of MgO was coated on the fcc-FePt nanoparticle (see Fig. S2†). Fct-FePt/MgO nanoparticles were obtained after annealing and were then acid-dipped to remove MgO and obtain fct-FePt nanoparticles. As can be seen from Fig. 1(a) and (b), fct-FePt nanoparticles are irregular spherical shapes and have an average size of about 11 nm. It should be pointed out that the
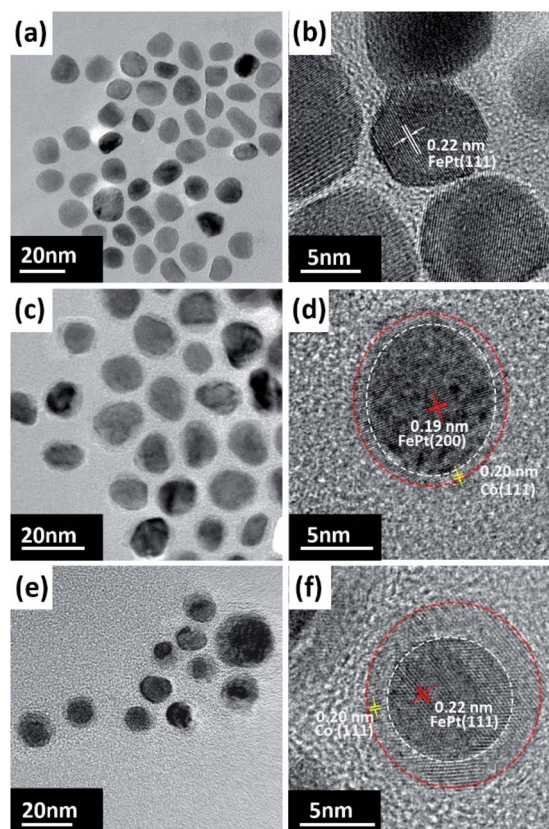

Fig. 1 TEM and HR-TEM images of (a), (b) L1$_0$-FePt nanoparticles, and the core–shell nanoparticles with (c), (d) 1 nm and (e), (f) 2.2 nm Co shell. The *d*-spacings are marked according to the indicated phases, L1$_0$-FePt (red), Co (white).

size of nanoparticles is smaller than the single-domain critical size of FePt alloys (about 340 nm). The HRTEM image of fct-FePt nanoparticles in Fig. 1(b) shows complete and transparent lattice fringes with the fringe spacing of 0.22 nm, matching the standard lattice spacing 0.22 nm of (111) planes for $L1_0$-FePt. The XRD patterns, as shown in Fig. S3,† also suggest the synthesis of $L1_0$-FePt. These facts indicate that the prepared nanoparticles are single crystal and single domain $L1_0$-FePt nanoparticles.

$L1_0$-FePt/Co core–shell nanoparticles were synthesized by the seed-mediated method. The precursor $Co(acac)_2$ was added and acted as the Co source. The thickness of the Co layer was determined by the addition amount of $Co(acac)_2$. Fig. 1(c)–(f) shows the TEM and HRTEM photographs of fct-FePt/Co core–shell nanoparticles with different Co shell thicknesses. The elemental mapping of $L1_0$-FePt/Co in Fig. S4† suggests that the Co layer is coated on the $L1_0$-FePt core. The core–shell structures are revealed by contrast difference between the center and the edge of nanoparticles in Fig. 1(c) and (e). The marked fringes spacing of the shells in Fig. 1(d) and (f) are 0.21 nm, corresponding to the interplanar spacing of fcc-Co (111) planes, while the core of 0.22 nm is corresponding to $L1_0$-FePt (111). Also, straight fringes indicate that the Co shell is epitaxial on the core surface.

The amount of $Co(acac)_2$ was taken as a variable to prepare different $L1_0$-FePt/Co core–shell nanoparticles. Four samples with the amount of $Co(acac)_2$ of 3 mg, 5 mg, 11 mg, and 12.5 mg were labelled as S_3, S_5, S_{11}, and $S_{12.5}$, respectively. In contrast, the $L1_0$-FePt nanoparticles were denoted as S_0. TEM images of sample S_5 and $S_{12.5}$ are shown in Fig. 1(c)–(f), where the thicknesses of Co shells were measured to be 1.4 nm and 2 nm. The Co shell thickness was a function of the amount of $Co(acac)_2$, and the calculated results are listed in Table 1.

$L1_0$-FePt/Co nanoparticle-based exchange-coupled magnets were prepared by fixing the core–shell nanoparticles in epoxy resin, where nanoparticles were fully dispersed in epoxy to avoid performance deterioration caused by agglomeration. The hysteresis loops of the samples measured at 300 K are shown in Fig. 2. $L1_0$-FePt nanoparticles without any Co coated layer exhibit typical hard magnetic performance (Fig. 2(a)), where the coercivity H_c reach up to 23.9 kOe and the saturation magnetization M_s is 32.1 emu g^{-1}.

For the core–shell nanoparticles, the H_c reduces with the increase of Co thickness while the M_s is improved, as shown in

Fig. 2(a)–(e), where the hysteresis loop changes from a typical hard type (Fig. 2(a)) to a soft type (Fig. 2(e)). Although the magnetic properties have changed, the hysteresis loops are still smooth and continuous, which could account for that the nanoparticles behave as a single-phase characteristic, demonstrating the good coupling between the $L1_0$-FePt cores and Co shells.[35] The $(BH)_{max}$ of S_3 with a thin Co shell is 4.9 GMOe, 48% higher than that of sample S_0 of 3.3 GMOe. However, magnetic properties of $L1_0$-FePt/Co core–shell nanoparticles deteriorate when the Co shells are too thick. For example, the $(BH)_{max}$ decreases from 4.6 GMOe of S_5 to 2.4 GMOe of $S_{12.5}$.

Anisotropic exchange-coupled $L1_0$-FePt/Co nano-magnets were prepared by orienting nanoparticles under an external magnetic field, in which OAm and OA were added to increase the dispersibility. After the epoxy solidified, the easy axes of nanoparticles would be aligned to the magnetic field direction as schematically shown in Fig. S1.†

The hysteresis curves of anisotropic nano-magnets were shown in Fig. 2(f)–(j). The orientated samples made by nanoparticles with different Co thicknesses were correspondingly labelled as S_0', S_3', S_5', S_{11}', $S_{12.5}'$. The coloured curves and grey curves in Fig. 2 were obtained by loading the measuring magnetic field parallel to and perpendicular to the easy axes of nanoparticles, respectively. The distinction of the curves in Fig. 2(f) intuitively demonstrated that the magnet has a significant anisotropy, a sign of successful orientation. When the nanoparticles were coated with a Co shell (sample S_3'), the H_c declined slightly, and the M_s increased, as shown in Fig. 2(g). Meanwhile, the distinction between the two curves was still evident, indicating the good orientation of $L1_0$-FePt/Co core–shell nanoparticles. Nanoparticles with thicker Co shells exhibited gradually decreasing H_c and increasing M_s. These two curves gradually coincide as the Co shells getting thicker, indicating the magnets tend to be isotropic.

Fig. 3 plots the magnetic properties of exchange-coupled $L1_0$-FePt/Co nano-magnets. The degree of orientation (V_1/V_2) of uniaxial permanent magnetic nanoparticles is closely related to the remanence ratio (M_r/M_s) as expressed by the equation $V_1/V_2 = 2M_r/M_s - 1$. As shown in Fig. 3(c), the aligned samples exhibit bigger M_r/M_s than the random ones due to the high degree of orientation. However, M_r/M_s declines dramatically with increasing Co shell thickness because the orientation becomes difficult as the Co shell is thick. As shown in Fig. 3(d), the $(BH)_{max}$ of both kinds of samples increases first and then decreases with Co layer thickness. It is well known that $(BH)_{max}$ is determined by two factors, namely M_s and H_c. On the one hand, when the Co shell is thin, the increase of M_s is dominant, which leads to an increase in $(BH)_{max}$. On the other hand, H_c goes down rapidly with the increase of Co thickness, leading to decreased $(BH)_{max}$. Furthermore, the $(BH)_{max}$ of the orientated samples is significantly higher than that of the random sample. The $(BH)_{max}$ of the oriented sample with a Co layer of 1 nm (S_5') reaches 7.16 GMOe, more than twice as high as 3.3 GMOe of the sample without orientation and Co shells. The $(BH)_{max}$ of sample S_0', S_3', S_{11}' and $S_{12.5}'$ are 5.88, 6.95, 5.45 and 2.2 GMOe, respectively, which suggests that sample S_5' has the largest $(BH)_{max}$. This is because the increase of Co thickness can

Table 1 The amount of Co precursor ($Co(acac)_2$) added to the samples and the corresponding Co thickness n and mass percentage M_{Co}/M

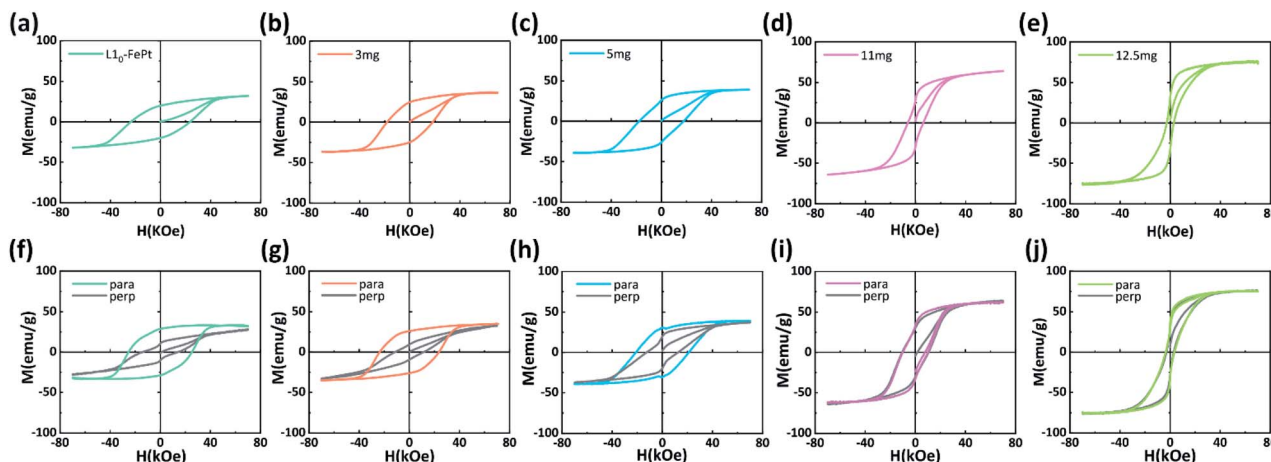| Sample	$Co(acac)_2$ added, mg	Thickness n, nm	M_{Co}/M, %
S_0	0	0	0
S_3	3	0.6	9
S_5	5	1	17
S_{11}	11	2	30
$S_{12.5}$	12.5	2.2	33

Fig. 2 Hysteresis loops measured at 300 K of samples with different Co(acac)$_2$. (a–e) Isotropic samples. (f–j) Oriented samples.
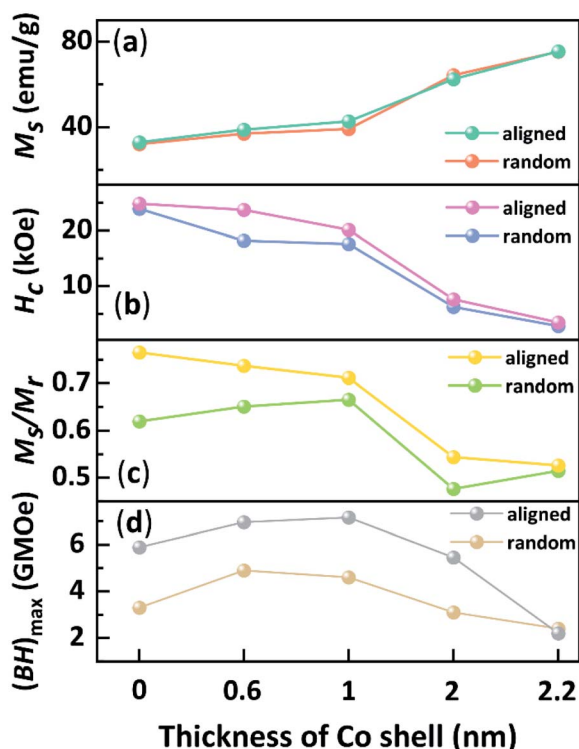

Fig. 3 Plotted curves of H_c, M_s, M_r/M_s, and $(BH)_{max}$ of exchange-coupled nano-magnets with different Co thickness.

$$K_{eff} = \int \varphi^*(r) K_1(r) \varphi(r) dr = \langle K_1(r) \rangle = f_s K_s + f_h K_h \qquad (1)$$

where f_s and f_h represent the proportion of soft and hard magnetic phases, respectively. K_s and K_h are the magnetic anisotropy constants of the soft and hard phases. K_{eff} could be calculated using the data in Table 1 according to eqn (1). Besides, the experimental effective magnetic anisotropy constants K'_{eff} of the unoriented samples could be calculated by the following formula,[36]

$$K'_{eff} = 2\varepsilon_0 H_c M_s \qquad (2)$$

Here, the ε_0 is the permeability of the vacuum. To compare the K_{eff} and K'_{eff}, K_{eff}/K_0 and K'_{eff}/K'_0 are plotted in Fig. 4, where K_0 and K'_0 are the theoretical and experimental effective magnetic anisotropy constants of the pure L1$_0$-FePt nano-magnet, respectively. The K_{eff}/K_0 linearly decreases with the increase of the Co shell thickness, while the variation of the experimental K'_{eff}/K'_0 can be divided into two stages. At stage I, when t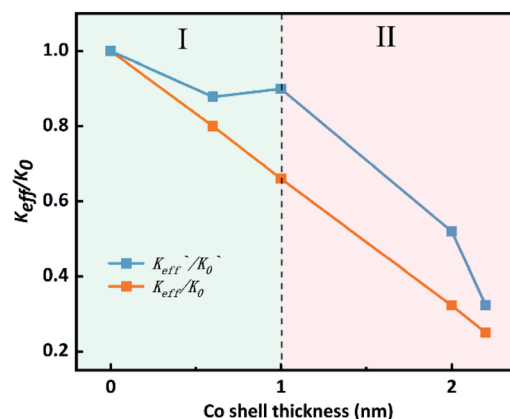he Co shell thickness is less than 1 nm, the practical increase the $(BH)_{max}$, but after a certain point, further increase in Co thickness will lead to orientation difficulties, and the increase of Co itself will seriously deteriorate the coercivity, resulting in a decrease in $(BH)_{max}$. Therefore, when the Co layer thickness is 1 nm, the performance of the sample exceeds 0.6 nm, 2 nm and 2.2 nm.

Based on the theoretical model of exchange-coupled magnets proposed by Skomski and Coey,[14] the theoretical effective magnetic anisotropy constants K_{eff} of the isotropic samples could be expressed by the following formula,

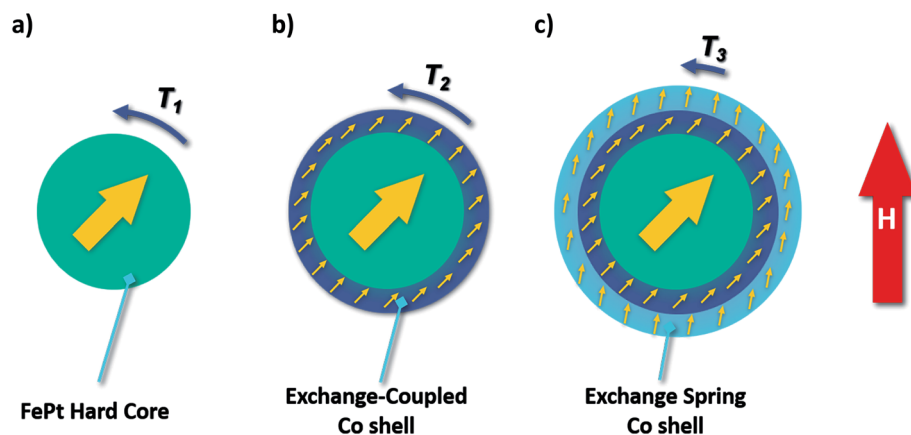**Fig. 4** The variation trend of the normalized effective anisotropy constant.

Fig. 5 Schematic diagram of the orientation process of core–shell nanoparticles.

K'_{eff}/K'_0 falls more slowly than the theoretical K_{eff}/K_0. This can be interpreted as the soft Co shell was hardened by the hard L1$_0$-FePt core through an intense exchange coupling effect. At stage II, the slop of K'_{eff}/K'_0 curve was equal to or less than K_{eff}/K_0, illustrating the anisotropy of samples decreases more quickly than the theoretical prediction because the newly added Co shells can no longer be hardened by the hard L1$_0$-FePt core.

Fig. 5 schematically shows one model of the phenomenon above. When the Co shell is very thin, strong magnetic hardening occurs, resulting in a slight decrease in the anisotropy. As the Co thickness grows, the Co shells transform into two layers with different coupling modes with the core. When the Co thickness exceeds 1 nm, the outer sphere becomes spring-exchange-coupled (Fig. 5(c)) instead of hard-exchange-coupled with the core (Fig. 5(b)), where hard-exchange-coupling and spring-exchange-coupling refers to the uniform rotation of the magnetic moment and the rotation of the magnetic moment in the soft phase that drives part of the hard phase to rotate, respectively.[24] The orientation pattern of the samples will change with the increase of Co thickness as applying an external magnetic field. Coherent rotation is known as the motion mode of single-domain nanoparticles in a magnetic field (Fig. 5(a)). A thin Co shell does not affect this rotation mode, and the Co shell can be considered to be co-phased with the core due to the pinned effect of exchange-coupling (Fig. 5(b)). Hence, the torque of orientation T_1 and T_2 should be the same. A thicker layer of Co shell leads to an exchange-spring effect between the outer and core layers (Fig. 5(c)). The constraint on the outer layers is reduced, and the magnetic moment of the outer layer rotates in advance so that the intersection angle between the magnetic moment and the magnetic field becomes small under the external magnetic field. Therefore, the torque T_3 is smaller than T_1 and T_2, which is consistent with the above conclusion that the thicker the Co shell, the more difficult the orientation.

Conclusions

In summary, magnetic L1$_0$-FePt nanoparticles were synthesized by a wet chemical method. Co shells with thickness ranging from 0.6 to 2.2 nm were successfully coated on the L1$_0$-FePt nanoparticles. Due to the exchange-coupled effect, the H_c monotonically decreased while the M_s increased with increasing Co thickness. When the Co shell was 1 nm thick, the $(BH)_{\text{max}}$ of the anisotropic magnets was increased by more than 80% with increased remanence and the substantially unchanged H_c. The Co thickness affects the proportion of the soft phase and hence the anisotropy constant. A thin Co shell tinily reduces the anisotropic constant, while a thicker Co, more than 1 nm, rapidly lowers the anisotropic constant. Meanwhile, when the Co shell becomes thick, the outer layer is no longer stringently controlled by the core. Hence, the magnetic moment in the outer shell is easily deflected by the external magnetic field, and the orientation was not complete. The anisotropic exchange-coupled nanoparticles built by a hard core and a soft shell are of much concern to the high-performance permanent magnets. This work focuses on the orientation of the hard-soft exchange-coupled nanoparticles, which is essential to prepare the next generation of high-performance permanent magnets.

Conflicts of interest

There are no conflicts to declare.

Acknowledgements

References

1 F. Liu, Y. Hou and S. Gao, *Chem. Soc. Rev.*, 2014, **43**, 8098–8113.

2 O. Gutfleisch, M. A. Willard, E. Brueck, C. H. Chen, S. G. Sankar and J. P. Liu, *Cheminform*, 2011, **42**, 1–22.

3 K. T. Chau, C. C. Chan and C. Liu, *IEEE Trans. Ind. Electron.*, 2008, **55**, 2246–2257.

4 A. M. El-Refaie, *IEEE Trans. Ind. Electron.*, 2010, **57**, 107–121.

5 J. M. D. Coey, *Scr. Mater.*, 2012, **67**, 524–529.

6 R. Skomski, P. Manchanda, P. K. Kumar, B. Balamurugan and D. J. Sellmyer, *IEEE Trans. Magn.*, 2013, **49**, 3215.

7 D. Li, Y. Li, D. S. Pan, Z. D. Zhang and C. J. Choi, *J. Magn. Magn. Mater.*, 2019, **469**, 535–544.

8 A. Kirkeminde, J. Shen, M. G. Gong, J. Cui and S. Q. Ren, *Chem. Mater.*, 2015, **27**, 4677–4681.

9 B. Balamurugan, B. Das, W. Y. Zhang, R. Skomski and D. J. Sellmyer, *J. Phys.: Condens. Matter*, 2014, **26**, 064204.

10 O. Gutfleisch, M. A. Willard, E. Bruck, C. H. Chen, S. G. Sankar and J. P. Liu, *Adv. Mater.*, 2011, **23**, 821–842.

11 A. D. Volodchenkov, Y. Kodera and J. E. Garay, *J. Mater. Chem. C*, 2016, **4**, 5593–5601.

12 B. Balamurugan, B. Das, V. R. Shah, R. Skomski, X. Z. Li and D. J. Sellmyer, *Appl. Phys. Lett.*, 2012, **101**, 5.

13 E. Lottini, A. Lopez-Ortega, G. Bertoni, S. Turner, M. Meledina, G. Van Tendeloo, C. D. Fernandez and C. Sangregorio, *Chem. Mater.*, 2016, **28**, 4214–4222.

14 R. Skomski and J. M. Coey, *Phys. Rev. B: Condens. Matter Mater. Phys.*, 1993, **48**, 15812–15816.

15 A. Figuerola, A. Fiore, R. D. Corato, A. Falqui, C. Giannini, E. Micotti, A. Lascialfari, M. Corti, R. Cingolani, T. Pellegrino, P. D. Cozzoli and L. Manna, *J. Am. Chem. Soc.*, 2008, **130**, 1477–1487.

16 S. Sun, C. B. Murray, D. Weller, L. Folks and A. Moser, *Science*, 2000, **287**, 1989–1992.

17 K. E. Elkins, T. S. Vedantam, J. P. Liu, H. Zeng, S. H. Sun, Y. Ding and Z. L. Wang, *Nano Lett.*, 2003, **3**, 1647–1649.

18 Y. Yu, L. He, J. Xu, J. Li and Y. Hou, *Nano Res.*, 2021, 1–6.

19 X. Liu, H. Wang, S. Zuo, T. Zhang, Y. Dong, D. Li and C. Jiang, *Nanoscale*, 2020, **12**, 7843–7848.

20 Y. Tamada, S. Yamamoto, S. Nasu and T. Ono, *Phys. Rev. B: Condens. Matter Mater. Phys.*, 2008, **78**, 214428.

21 F. Casoli, P. Lupo, L. Nasi, R. Cabassi, S. Fabbrici, F. Bolzoni, P. Ranzieri and F. Albertini, *J. Appl. Phys.*, 2015, **117**, 3588–3317.

22 H. Zeng, J. Li, J. P. Liu, Z. L. Wang and S. H. Sun, *Nature*, 2002, **420**, 395–398.

23 F. Liu, J. Zhu, W. Yang, Y. Dong, Y. Hou, C. Zhang, H. Yin and S. Sun, *Angew. Chem., Int. Ed. Engl.*, 2014, **53**, 2176–2180.

24 D. J. Carnevale, M. Shatruk and G. F. Strouse, *Chem. Mater.*, 2016, **28**, 5480–5487.

25 D. Li, H. Wang, Z. Ma, X. Liu, Y. Dong, Z. Liu, T. Zhang and C. Jiang, *Nanoscale*, 2018, **10**, 4061–4067.

26 W. Yang, W. Lei, Y. Yu, W. Zhu, T. A. George, X. Z. Li, D. J. Sellmyer and S. Sun, *J. Mater. Chem. C*, 2015, **3**, 7075–7080.

27 M. Pousthomis, C. Garnero, C. G. Marcelot, T. Blon, S. Cayez, C. Cassignol, V. A. Du, M. Krispin, R. Arenal, K. Soulantica, G. Viau and L. M. Lacroix, *J. Magn. Magn. Mater.*, 2017, **424**, 304–313.

28 W. Zhang, W. B. Yang, R. U. Chandrasena, V. B. Ozdol, J. Ciston, M. Kornecki, S. Raju, R. Brennan, A. X. Gray and S. Q. Ren, *Chem. Commun.*, 2018, **54**, 11005–11008.

29 S. J. A. Figueroa, S. J. Stewart, T. Rueda, A. Hernando and P. de la Presa, *J. Phys. Chem. C*, 2011, **115**, 5500–5508.

30 Y. Chai, F. Feng, Q. Li, C. Yu, X. Feng, P. Lu, X. Yu, M. Ge, X. Wang and L. Yao, *J. Am. Chem. Soc.*, 2019, **141**, 3366–3370.

31 A. López-Ortega, M. Estrader, G. Salazar-Alvarez, A. G. Roca and J. Nogués, *Phys. Rep.*, 2015, **553**, 1–32.

32 Q. Li, L. Wu, G. Wu, D. Su, H. Lv, S. Zhang, W. Zhu, A. Casimir, H. Zhu, A. Mendoza-Garcia and S. Sun, *Nano Lett.*, 2015, **15**, 2468–2473.

33 J. Kim, C. Rong, Y. Lee, J. Ping Liu and S. Sun, *Chem. Mater.*, 2008, 7242–7245.

34 J. Kim, C. Rong, J. P. Liu and S. Sun, *Adv. Mater.*, 2009, **21**, 906–909.

35 S. H. Moon, S. H. Noh, J. H. Lee, T. H. Shin, Y. Lim and J. Cheon, *Nano Lett.*, 2017, **17**, 800–804.

36 J. Arcas, A. Hernando, J. M. Barandiarán, C. Prados and A. Neuweiler, *Phys. Rev. B: Condens. Matter Mater. Phys.*, 1998, **58**, 5193–5196.